Computational Screening of Indirect-Gap Semiconductors for Potential Photovoltaic Absorbers

Youngho Kang,*[,†] Yong Youn,[‡] Seungwu Han,[‡] Jiwon Park,[†] and Chang-Seok Oh[†]

[†]Materials Data Center, Korea Institute of Materials Science, Changwon 51508, Korea

[‡]Department of Materials Science and Engineering, Seoul National University, Seoul 08826, Korea

S Supporting Information

ABSTRACT: Photovoltaic (PV) absorbers are key components of PV cells used to harvest solar energy, which is an attractive renewable energy resource. In this study, a high-throughput computational screening is conducted to discover potential PV absorbers. While direct-gap semiconductors are usually favored as PV absorbers, herein, we focus on indirect-gap semiconductors that could exhibit a long lifetime of photocarriers because of the low probability of band-to-band recombination, enabling high-performance PV cells. From the Materials Project database, we screen semiconductors considering the direct band gap, the difference between the direct and indirect band gaps, and the effective mass of carriers as selection metrics. Taking low costs and earth abundance of constituent elements into account, we suggest $GeAs_2$, $SiAs_2$, and $NaSbS_2$ as particularly promising indirect-gap semiconductors. Their absorption and defect properties are analyzed in detail, providing a route to engineering materials with high efficiency.
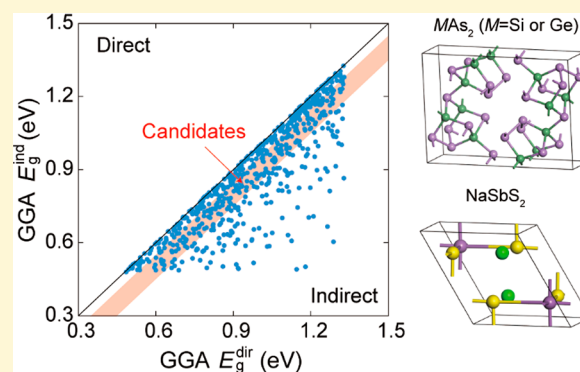
1. INTRODUCTION

The unprecedented increase in human population over the past few decades has led to massive consumption of fossil fuels such as coal, oil, and natural gas to meet the growing demands for energy. Unfortunately, fossil fuels are nonrenewable resources that take millions of years to form but cannot be readily restocked once exhausted. Furthermore, burning fossil fuels results in emission of greenhouse gases, such as carbon dioxide (CO_2), thus exacerbating global warming. To overcome these drawbacks associated with fossil fuels, significant efforts have been put into developing technologies to harvest eco-friendly renewable energy resources such as solar, wind, and geothermal energy.[1]

Among various types of known renewable energy resources, solar energy is particularly appealing due to its wide availability as well as facile transformation into electricity through photovoltaic (PV) cells. The performance of a PV cell depends on the material that absorbs photons to generate electron and hole carriers and deliver photogenerated carriers to the outer circuit.[2−4] Currently, Si is widely used as a PV absorber because of its abundance on earth and low costs. Moreover, technologies to process Si are already well developed.[5] However, despite its favorable band gap (∼1.1 eV), Si poorly absorbs visible light due to the indirect nature of the gap. Consequently, thick Si wafers are required to absorb light over broad frequencies above the band gap, which degrades power conversion efficiency (PCE) due to enhanced nonradiative recombination and increases the cost of Si solar cells.[4] On the other hand, direct-gap semiconductors such as GaAs[6] and

Cu(In,Ga)(Se,S)$_2$ (CIGS)[7] have better absorption properties than Si, but they are made of expensive elements such as In and Ga.[4,6] As such, their application is limited to niche markets where efficiency is the foremost concern. Recently, halide perovskites such as methylammonium lead iodine ($CH_3NH_3PbI_3$) have emerged as an exciting class of semiconductors for application as PV absorbers.[8−10] Interestingly, in spite of short research history, the efficiency of perovskite-based PV cells is comparable to those of traditional PV cells.[11] However, halide perovskites suffer from various thermodynamic and chemical instabilities associated with organic molecules, which impedes commercialization of PV cells based on these materials.[12,13]

As discussed in the above, currently known PV absorbers have their own disadvantages, and thus new materials that are free from such drawbacks are in demand. In this study, to discover new interesting PV absorbers, we screen physical properties of semiconductors by exploring a large publicly available computational database and performing additional high-throughput first-principles calculations. There exist several studies on identifying efficient PV absorbers via high-throughput computational screening.[14−17] In those works, indirect-gap semiconductors were not paid attention as much as direct-gap materials because of weak absorption of light. However, recent works on perovskite-based solar cells indicate

that the indirect nature of the band gap retards band-to-band recombination, which can positively affect PCE of the PV cell.[18,19] Motivated by these observations, in the present work, we focus on indirect semiconductors. We screen 56447 inorganic materials whose band structures are provided in the Materials Project (MP) database.[20] By considering the direct band gap, difference between the direct and indirect band gaps, and the effective mass, we select 31 candidates. When the earth abundance and material cost are taken into account, we find that $GeAs_2$, $SiAs_2$, and $NaSbS_2$ are particularly promising. The computed absorption coefficients confirm that these indirect-gap semiconductors absorb visible light efficiently. By further studying native defects, we provide guidelines to optimize growth conditions that can minimize efficiency loss due to defects.

2. METHODOLOGY

2.1. Effective Mass Calculation. The effective mass tensor of semiconductors is obtained through the Boltzmann transport theory with a constant relaxation time.[21,22] To this end, we carry out first-principles calculations using the Vienna *Ab-Initio* Simulation Package (VASP) code within the PAW formalism.[23,24] We use the PBE functional to calculate the exchange-correlation potential.[25] The cutoff energy of plane wave basis is automatically controlled by setting the PREC tag in the VASP code as "High". The atomic structures of the target materials are obtained from the MP database.[20] The Boltzmann transport calculation requires a very fine k-point mesh to ensure a satisfactory convergence of results. Thus, the band structure that is obtained on a coarse k-point grid is interpolated on a finer k-point grid using the Fourier transformation employing BoltzTrap2.[26]

2.2. Hybrid Functional Calculations. We use the HSE06 functional with 25% mixing of the exact-exchange energy.[27,28] The cutoff energy of the plane wave basis is set to 300 eV, and the k-point mesh is adjusted to ensure energy convergence within 10 meV/atom. The atomic structure is relaxed until forces acting on each atom become <0.05 eV/Å. In the case of layered materials, we consider van der Waals interactions using the approach proposed by Grimme et al.[29]

2.3. Optical Absorption Coefficient. To obtain the optical absorption spectrum, we initially evaluate the imaginary part of dielectric functions (ϵ_2) within the independent-particle approximation using PBE, and the real part (ϵ_1) is obtained by the Kramers−Kronig transformation of ϵ_2. The optical absorption coefficient is then computed as follows:

$$\alpha_{ij} = \frac{2\omega}{c} \sqrt{\frac{\sqrt{\epsilon_{1,ij}^2 + \epsilon_{2,ij}^2} - \epsilon_{1ij}}{2}} \tag{1}$$

where ω and c are the photon frequency and speed of light, respectively. i and j in eq 1 denote the Cartesian axis. By applying the scissor operator, we rigidly shift the calculated absorption spectrum to match the direct band gap obtained from the HSE06 calculations. The validity of this scissor-operator approximation was verified in an earlier work.[30]

3. RESULTS

3.1. Design of PV Absorbers. *3.1.1. Target Material Properties.* The performance of a PV cell is measured by its maximum PCE (η_{max}):[2]

$$\eta_{max} = \frac{I_{SC} V_{OC} FF}{P_{in}} \tag{2}$$

where I_{SC} is a short-circuit current (photogenerated current through an external circuit at zero bias) and V_{OC} is the open-circuit voltage at which the current does not flow along the circuit, which corresponds to the highest voltage that the PV cell can produce. I_{SC} and V_{OC} are the intrinsic figures of merit of the PV cell. In eq 2, FF is the fill factor which is a measure of PV cell quality, and P_{in} is the input power from incident light.

Shockley and Queisser (S−Q) derived the thermodynamic limit of η_{max} for a single p−n junction PV cell as a function of the band gap (E_g) of semiconductors using the detailed balance.[31] (In this work, E_g means the fundamental band gap, referring to the smallest difference in energies between conduction and valence bands, regardless of its nature.) According to their theory, the best PV absorber has E_g of 1.3 eV with η_{max} of 33%. Such an optimal band gap results from opposing dependences of I_{SC} and V_{OC} on E_g; the large band gap increases V_{OC} but reduces I_{SC} by suppressing absorption of sunlight. However, many materials with E_g close to 1.3 eV exhibit poor η_{max},[4] implying that E_g alone is insufficient as a metric for material selection.

To identify material properties that are necessary for selecting potential PV absorbers, we examine the light-to-electricity conversion process in Figure 1. Upon illumination
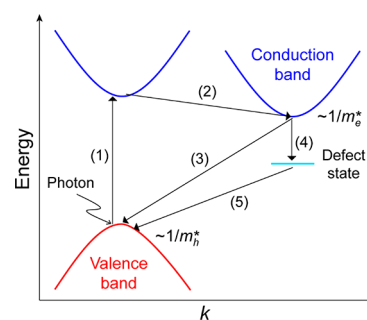

Figure 1. Dynamic processes occurring in PV absorbers: (1) light absorption, (2) thermalization, (3) band-to-band recombination, and defect-induced (4) electron and (5) hole trapping.

with light with photon energies above the band gap, electrons and holes are generated in semiconductors [path (1) in Figure 1] and carry photocurrents. Thus, strong optical absorption is essential to increase I_{SC}. Because indirect transitions are inefficient compared to direct ones, good absorbers should have a direct band gap (E_g^{dir}) optimal for strong absorption of photons in the visible range.

Electron (hole) carriers created by absorbing high-energy photons initially occupy high-energy states in conduction (valence) bands. These hot carriers lose excess energies via electron−phonon interactions, which is called thermalization. Such thermalization processes occur within tens of femtoseconds, which is much faster than recombination processes.[32] Thus, carriers relax down to band edges [path (2) in Figure 1] before recombination.

To convert into currents through the outer circuit, photocarriers should diffuse and arrive at electrodes. Therefore, a large diffusion length of photocarriers is beneficial for achieving high I_{SC}. This means that recombination of photocarriers, which determines the carrier lifetime, should be suppressed. In addition, recombination adversely affects

V_{OC} which corresponds to the splitting of quasi-Fermi levels of electrons and holes under illumination; a short carrier lifetime due to recombination weakens splitting by reducing the number of photocarriers occupying the valence and conduction bands in the steady state.[33] Among several recombination mechanisms, crucial are band-to-band radiative recombination [path (3) in Figure 1] and defect-induced recombination [paths (4) and (5) in Figure 1 for electron and hole traps, respectively], which is also called the Shockley–Read–Hall (SRH) recombination.[34−36] In suppressing band-to-band recombination, the indirect gap would be beneficial because the indirect transition is less probable than direct one. On the other hand, the SRH recombination is mostly nonradiative, and its rate increases significantly with defect concentrations. Here the energy level of the defect state is another important factor determining the SRH recombination rate; defects with levels near the midgap are likely to be more active than others with levels close to band edges because of moderate capture rates for both electron and hole carriers.[37,38] As a result, PV absorbers should have low defect concentrations, particularly of defects generating midgap levels.

Lastly, good transport properties are necessary for the facile extraction of photocarriers. According to the Drude model, the carrier mobility is inversely proportional to the effective mass, and therefore small effective masses in both valence and conduction bands are desirable.

3.1.2. Computational Screening. The overall workflow used for screening is present in Figure 2. To find potential PV
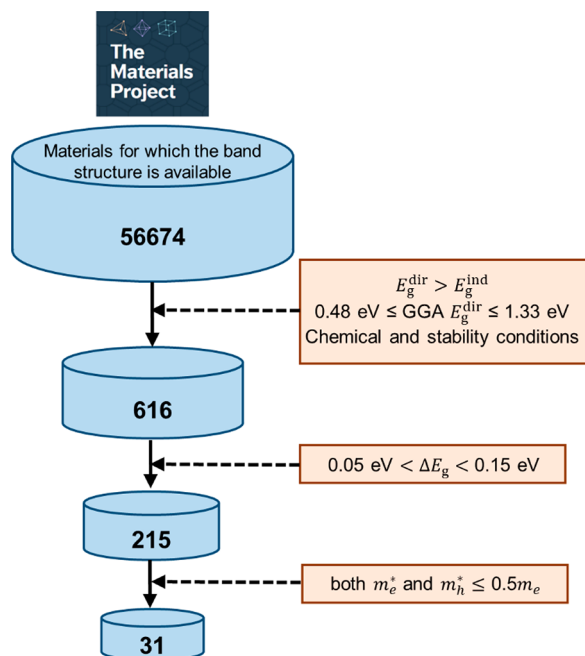

Figure 2. Workflow of screening for PV absorbers with indirect gaps.

absorbers possessing both low band-to-band recombination rates and strong absorption of the visible light, we begin with searching the MP database[20] for indirect semiconductors with E_g^{dir} between 0.8 and 1.9 eV. According to the S−Q criteria, this range of E_g^{dir} ensures that the theoretical limit of η_{max} is higher than 25% when $E_g^{dir} = E_g$. In addition, this condition of the direct band gap would allow the strong absorption of visible light, thereby alleviating the requirement of a large thickness of absorbers. As the generalized gradient approx-

imation (GGA) that was used to produce band structures in the MP underestimates the band gap of semiconductors by 30%−40%,[39] we consider factors of 0.6 and 0.7 for the lower and upper bounds of the target range of E_g^{dir}, respectively, when selecting PV absorber materials. That is to say, we select materials satisfying 0.48 eV ≤ GGA E_g^{dir} ≤ 1.33 eV. Herein, we filter out materials that are predicted to be thermodynamically unstable or decompose into other phases by removing materials with the positive enthalpy of formation or convex hull value in the MP database. Semiconductors including 3d transition metals (Sc, V, Cr, Mn, Fe, Co, and Ni) are also excluded as they typically exhibit large effective masses due to the strongly localized nature of 3d states.[21] We limit the maximum number of constituent elements to three because diverse composition may increase the efforts required to optimize growth conditions.

From the initial screening of 56447 inorganic materials for which the MP database provide the band structure, we identify 616 materials, and the distribution of their band gaps is shown in Figure 3. Note that all the screened materials lie in the
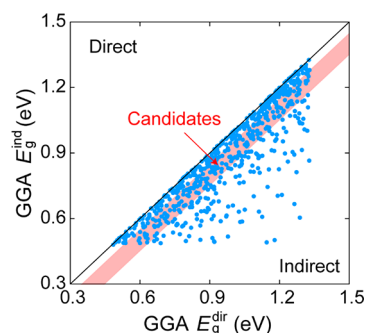

Figure 3. Distribution of direct and indirect band gaps obtained using GGA calculations on 617 indirect-gap semiconductors chosen from the initial screening (see the main text). The region where 0.05 eV < $E_g^{dir} - E_g^{ind}$ < 0.15 eV is shaded in red.

lower-right triangle because the band gap is indirect [$E_g^{dir} > E_g^{ind}$ (indirect band gap)]. For the next stage of screening, we apply a boundary condition to the band-gap difference $\Delta E_g = E_g^{dir} - E_g^{ind}$. If ΔE_g is too small, direct band-to-band recombination would be still significant because of thermal effects. Therefore, we set the lower limit of ΔE_g to 0.05 eV. On the other hand, because V_{OC} scales with E_g, a large ΔE_g would undermine V_{OC} even if the indirect nature may increase V_{OC} by retarding band-to-band recombination. A proper upper limit of ΔE_g can be determined via the following equation.[40]

$$qV_{OC} = E_g - k_B T \ln\left(\frac{N_c N_v}{np}\right) \tag{3}$$

where q, k_B, and T are the electron charge, the Boltzmann constant, and temperature, respectively, $N_{c(v)}$ is the effective density of states in the conduction (valence) band, and n (p) denotes the concentration of the photoexcited electron (hole) carriers at quasi-equilibrium. As current is zero in the open-circuit condition, the generation rate ($G_{e−h}$) should be equal to the recombination rate ($R_{e−h}$). If the PV absorber has a high crystallinity or contains none of the defects with subgap states around the midgap, radiative recombination will be dominant such that $R_{e−h} = k_{rad}np$, where k_{rad} is a bimolecular coefficient of radiative recombination. Under such conditions, the open-circuit condition can be written as follows:

$$G_{e-h} = k_{rad}np \tag{4}$$

Eliminating np in eq 3 using eq 4 leads to

$$qV_{OC} = E_g - k_B T \ln\left(\frac{k_{rad}N_cN_v}{G_{e-h}}\right) \tag{5}$$

Equation 5 clearly shows the advantage of small k_{rad} of indirect-gap materials when compared to direct-gap materials. For instance, direct-gap materials such as GaAs and CdTe have k_{rad} values of $\sim 10^{-10}$ cm^3/s, while the corresponding value is $\sim 4 \times 10^{-13}$ cm^3/s in weakly indirect-gap materials like $CH_3NH_3PbI_3$.[18] As a result, the loss in V_{OC} due to radiative recombination is smaller in the latter by ~ 0.14 V when all other parameters remain the same. However, as ΔE_g becomes larger, E_g decreases, which detrimentally affects V_{OC}. Therefore, ΔE_g should not be larger than a benefit in qV_{OC} arising from low band-to-band recombination rate.

This benefit of the indirect nature of the band gap was not noticed in previous screening studies using spectroscopic limited maximum efficiency (SLME), which extends the S−Q limit by considering the absorption spectrum and film thickness in the determination of the efficiency as a main selection metric.[15−17] In the SLME metric, the presence of lower indirect gaps is assumed to deteriorate V_{OC} of PV cells by increasing a chance of nonradiative recombination. However, as found by Bercx et al.,[41] applying the SLME metric to indirect-gap semiconductors is unfair, producing zero V_{OC} (as a result, zero PCE) of solar cells using Si, a prototype indirect-gap semiconductor widely used as a PV absorber. In experiments, Si solar cells were reported to retain substantial V_{OC} up to ~ 0.73 V, yielding $\sim 25\%$ of PCE, which corresponds to almost 70% of its E_g/q. This ratio, namely qV_{OC}/E_g, is comparable to those of solar cells employing direct-gap semiconductors (80% of GaAs, 65% of CIGS, and 58% of CdTe).[4] We think that nonradiative recombination loss cannot be simply estimated by the nature of the band gap. It is rather associated with other properties such as defects.

On the other hand, our justification of the range of ΔE_g for the screening, particularly the lower bound, is rather qualitative. Elaborate physical models to evaluate the recombination rate in consideration of the full electronic band structure as well as electron−phonon interactions and its impact on I_{SC} and V_{OC} should be developed to precisely determine the optimal range of ΔE_g.

On the basis of the foregoing discussions, we apply the condition of 0.05 eV $\leq \Delta E_g \leq 0.15$ eV to further narrow down the list of candidates (see shaded region in Figure 3), assuming that the band-gap difference is reliable in the GGA calculations used for screening. (It was shown by Yim et al. that the band structure shifts rigidly in most materials when the hybrid functional is used.[42]) This leads to a smaller group of candidates, including 215 semiconductors.

Next, we conduct high-throughput calculations to evaluate the effective masses of electron (m_e^*) and hole (m_h^*) for materials selected in the previous step. The effective mass is a tensor that may exhibit strong anisotropy, especially in the case of layered materials. Such anisotropic materials can be useful if the crystal direction is controlled properly. Therefore, to include them, we consider the lowest of the diagonal components. The results are displayed in Figure 4, which shows that m_h^* tends to be larger than m_e^*. The high PCE requires that both types of carriers exhibit good transport properties. This can be reflected in the screening process by
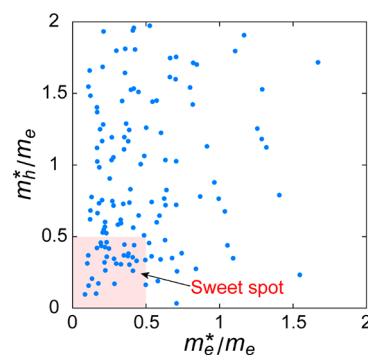

Figure 4. Distribution of the effective masses of electron and hole carriers of 215 indirect-gap semiconductors. The red-shaded region represents the sweet spot in which the effective masses of both electrons and holes are smaller than 0.5.

requiring that both m_e^* and m_h^* be smaller than $0.5m_e$, where m_e is the electron mass. We note that effective masses from GGA calculations tend to underestimate experimental values.[43] This means that materials with large GGA effective masses are hardly expected to exhibit the favorable transport properties although other factors such as scattering time also affect them. In Figure 4, we find that 31 candidates are included in the sweet spot and their properties, obtained using GGA calculations, are listed in Table 1 along with their MP id's. Note that traditional PV absorbers such as Si, GaAs, and CIGSs are not included in Table 1 because they do not meet the present band-gap criterion.

We used the direct band gap as a rough descriptor for the absorption properties for the screening. Even if we do not consider absorption spectra explicitly, most of materials excluded by the band-gap criteria would be less promising than the selected ones, regardless of the absorption strength above the gap due to opposing dependences of I_{SC} and V_{OC} on E_g.

Our computational screening relied on results from GGA calculations, which is a practical way we can choose with reasonably generous limits. There are more sophisticated approaches to predict optical and electrical properties such as the GW method, time-dependent DFT, and Bethe−Salpeter equations. However, these methods are computationally so demanding that they cannot be employed for screening over thousands of materials currently.

3.2. Promising Materials: SiAs$_2$, GeAs$_2$, and NaSbS$_2$. The materials present in Table 1 were selected by considering several physical properties relevant for a PV absorber. However, although such materials have potentials for high PCE of the PV cell, if the production is expensive and/or the constituent elements are scarce, such materials are difficult to be used as absorbers practically. Accordingly, the compounds including noble or rare-earth elements such as Ho$_2$TeO$_2$ and Ag$_3$SnP$_7$ are less attractive than the others. Furthermore, Table 1 contains several compounds like Ba(GeP)$_2$ and La$_{10}$Se$_{19}$ that have not been synthesized experimentally. Further investigations on the stability of such materials therefore are needed, even if they are predicted to be stable theoretically.

In light of the above discussions, GeAs$_2$, SiAs$_2$, and NaSbS$_2$ are of greater interest than the others because they consist of cheap and abundant elements and have been synthesized.[44,45] In the following subsections, we examine their absorption coefficient (α) as a function of the photon energy, which is a critical factor affecting PCE, noting that the dipole transition

Table 1. MP-id and Direct and Indirect Band Gaps as Well as the Lowest Component of the Electron and Hole Effective Mass Tensors of 31 Candidates Obtained by Using GGA Calculations (Values in Parentheses Represent the Harmonic Mean of the Effective Masses)

materials	MP-id	GGA E_g^{dir}	GGA E_g^{ind}	m_e^*	m_h^*
Tl_2SnTe_3	mp-28662	0.59	0.49	0.29 (0.45)	0.17 (0.32)
Ag_3SnP_7	mp-29849	0.63	0.51	0.23 (0.38)	0.36 (0.68)
$Ba(GeP)_2$	mp-27809	0.62	0.51	0.28 (0.33)	0.34 (0.36)
$BaGe_2$	mp-2139	0.63	0.53	0.41 (0.67)	0.26 (0.46)
$La_{10}Se_{19}$	mp-8866	0.69	0.58	0.38 (0.45)	0.36 (0.54)
Ho_2TeO_2	mp-768908	0.71	0.59	0.35 (0.39)	0.37 (0.53)
Tl_9SbTe_6	mp-34292	0.72	0.61	0.17 (0.21)	0.42 (0.46)
$Ca_3(GeAs_2)_2$	mp-18504	0.71	0.62	0.39 (0.63)	0.30 (0.44)
TlAgTe	mp-5874	0.69	0.64	0.23 (0.25)	0.46 (0.61)
Te_2Br	mp-27648	0.76	0.66	0.22 (0.51)	0.43 (0.70)
$NaBiSe_2$	mp-35015	0.80	0.71	0.11 (0.14)	0.16 (0.24)
$GeAs_2$	mp-17524	0.79	0.71	0.11 (0.18)	0.37 (0.68)
$RbAuBr_3$	mp-27300	0.81	0.73	0.35 (0.37)	0.44 (0.71)
Hg_2AsF_6	mp-540925	0.83	0.74	0.08 (0.25)	0.10 (0.28)
$Sr_3(GeAs_2)_2$	mp-17504	0.88	0.78	0.44 (0.64)	0.33 (0.55)
$LiBiS_2$	mp-33526	0.90	0.81	0.16 (0.23)	0.10 (0.15)
BeP_2	mp-27148	0.93	0.83	0.42 (0.48)	0.44 (0.44)
$Ca(ZnP)_2$	mp-9569	1.00	0.88	0.25 (0.34)	0.42 (0.46)
$CsAcTe_2$	mp-867341	1.01	0.88	0.38 (0.38)	0.38 (0.38)
$NaSbS_2$	mp-5414	0.98	0.88	0.10 (0.12)	0.31 (0.34)
$Sr_3(GeP_2)_2$	mp-18351	0.98	0.92	0.50 (0.81)	0.34 (0.61)
Cs_3Ge_4Au	mp-510341	1.06	0.93	0.50 (0.77)	0.16 (0.45)
Ga_2Te_5	mp-2371	1.01	0.96	0.19 (0.21)	0.46 (0.54)
K_2Te_2As	mp-29380	1.04	0.96	0.22 (0.54)	0.26 (0.68)
$CsTeSe_3$	mp-9462	1.03	0.98	0.30 (0.55)	0.31 (0.43)
Sr_4Sb_2O	mp-755293	1.11	0.98	0.20 (0.27)	0.43 (0.58)
NaMgSb	mp-7090	1.13	1.04	0.41 (0.43)	0.36 (0.48)
WBr_6	mp-28483	1.14	1.07	0.33 (0.37)	0.31 (0.35)
AlSb	mp-2624	1.28	1.23	0.22 (0.22)	0.32 (0.32)
Cs_2PtC_2	mp-505825	1.32	1.27	0.18 (0.41)	0.17 (0.51)
$SiAs_2$	mp-978553	1.03	0.88	0.13 (0.29)	0.21 (0.45)

above E_g^{dir} is not always guaranteed. For instance, In_2O_3 has the direct band gap of 2.9 eV, but the optical absorption effectively occurs above 3.7 eV because the dipole transitions below 3.7 eV are forbidden due to orbital symmetry.[46] We also investigate formation energies of point defects which can have a detrimental effect on PCE by acting as nonradiative recombination centers for photocarriers. The analysis on defects associated with nonradiative recombination may suggest optimal growth conditions that can help to reduce the concentration of such defects.

3.2.1. Absorption Coefficient. The crystal structures of MAs_2 (Figure 5a), where M = Ge or Si, and $NaSbS_2$ (Figure 5b) are based on the orthorhombic and monoclinic lattice, respectively (their band structures calculated by using the
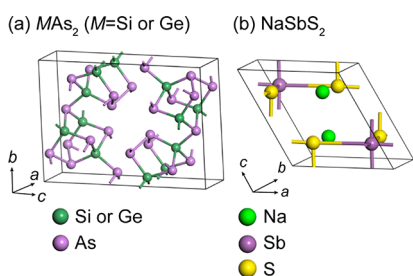
HSE06 hybrid functional are present in Figure S1). Figure 6 shows their absorption spectrum. Because of their structural anisotropy, the absorption coefficient slightly varies depending on the polarization axis of light. It is noted that the absorption coefficient starts to rise at the corresponding direct band gaps, indicating optical transition near the direct band gap is dipole-allowed in all of the three materials. As a result, the absorption of visible light is significant within absorption coefficients ranging over 10^4–10^5 cm^{-1}. Such magnitudes of absorption coefficient have been found in direct-band-gap semiconductors like GaAs, but an order of magnitude higher than that of Si.[47] However, the increment of absorption coefficients with respect to the photon energy is rather slow around the direct band gap in these materials, reaching 10^4 cm^{-1} above the absorption onsets by 0.1–0.3 eV depending on the polarization direction of light and materials. Nevertheless, the computed SLME (we assume the candidates are direct-gap semiconductors) indicates that they absorb sunlight enough to yield PCEs comparable with that of GaAs[17] (see Figure S2).

3.2.2. Point Defects. We calculate the defect formation energy (E^f) of native defects such as vacancies and self-interstitials as follows[48]

(a) MAs_2 (M=Si or Ge)   (b) $NaSbS_2$

Si or Ge
As
Na
Sb
S

Figure 5. Crystal structures of MAs_2 (M = Si or Ge) and $NaSbS_2$.

$$E^f[D^q] = E_{tot}[D^q] - E_{tot}[crystal] - \sum_i n_i\mu_i + qE_F + \Delta^q$$
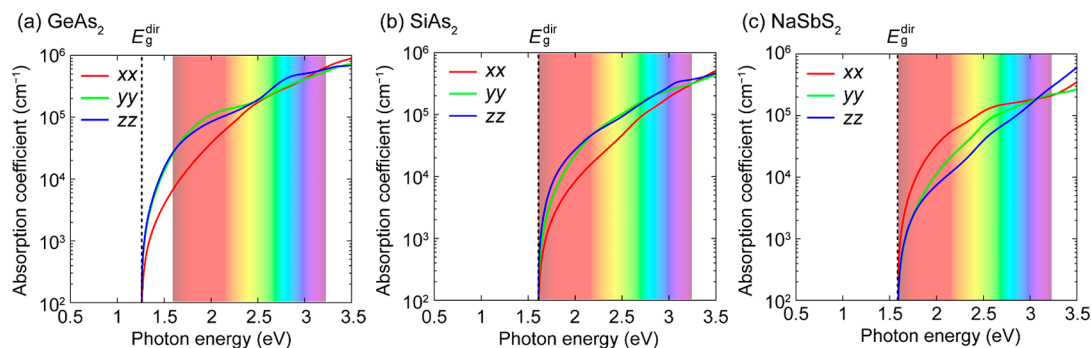
(6)

Figure 6. Absorption coefficient calculated with respect to photon energy of (a) GeAs$_2$, (b) SiAs$_2$, and (c) NaSbS$_2$. The notations *xx*, *yy*, and *zz* represent the polarization axes of light.

where $E_{tot}[D^q]$ and $E_{tot}[crystal]$ are the total energies of a supercell including a defect in charge state q and a perfect crystal, respectively, n_i is the number of atoms of type i that are removed from $(n_i < 0)$ or added to $(n_i > 0)$ supercells with the chemical potential of μ_i, and E_F denotes the Fermi level, referenced to the valence band maximum (VBM). In eq 6, the finite cell size correction, Δ^q, is applied following the scheme suggested by Freysoldt et al.[49,50] The boundary values for μ_i are determined by imposing conditions of the phase stability (see the Supporting Information for details about the determination of μ_i). To obtain reliable defect properties, we use the HSE06 functional that is known to produce accurate electronic and atomic structures of semiconductors.[27,28]

Figures 7a and 7b show the formation energies of native defects of GeAs$_2$ in As-poor and As-rich conditions, respectively. We only present the formation energy of defects in the stable charge state, which is indicated by the segment slopes in the formation-energy plot. Kinks in the curves correspond to transition levels between different charge states $[\varepsilon(q/q')]$. When $q' - q = 1$, $\varepsilon(q/q')$ represents a thermodynamic defect level whose energy position affects the overall SRH recombination rate.[37,38] In the crystalline structure of GeAs$_2$, there are two symmetrically nonequivalent sites for As. Thus, we provide two independent formation energy curves for the As vacancy (V_{As1} and V_{As2}).

We find that the Ge interstitial (Ge$_i$) has the lowest formation energy when the Fermi level lies below the center of the band gap, while V_{As2} does when the Fermi level is close to the conduction band minimum, regardless of growth conditions. These defects result in multiple defect levels in the band gap, as shown in Figure 8. In particular, the $\varepsilon(0/1+)$ and $\varepsilon(1+/2+)$ states of Ge$_i$ and $\varepsilon(2-/1-)$ and $\varepsilon(1-/0)$ states of V_{As2} lie at 0.3 eV above the midgap position. Therefore, they are expected to serve as efficient SRH recombination centers. To minimize the negative impact of these defects, GeAs$_2$ should be grown under As-rich conditions. In addition, maintaining the Fermi level near the midgap during growth will be helpful because both Ge$_i$ and V_{As2} have the high defect formation energies. We want to note that the Fermi level of undoped semiconductors is expected to lie around the midgap, but compound semiconductors sometimes have been grown with the Fermi levels near band edges due to unintentional doping by contaminants like hydrogen.[51,52] Therefore, it is necessary to avoid unintentional doping during the growth process.

In SiAs$_2$, Si interstitial (Si$_i$) and V_{As1} are expected to be the major defects when the Fermi level lies below and above the midgap, respectively (see Figure 7c for As-rich and Figure 7d
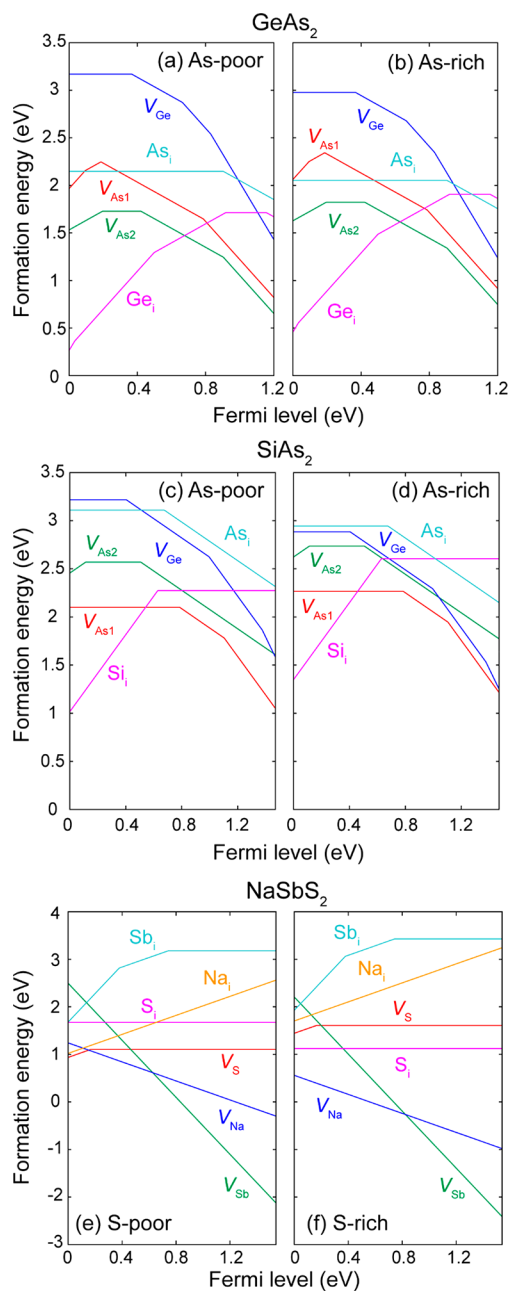

Figure 7. Defect-formation energies of native defects in GeAs$_2$, SiAs$_2$, and NaSbS$_2$ under anion-rich [(a), (c), and (e), respectively] and anion-poor [(b), (d), and (f), respectively] conditions.
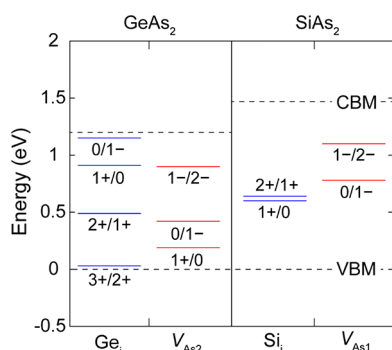
Figure 8. Charge transition levels between successive charge states of major defects in GeAs$_2$ and SiAs$_2$. VBM and CBM denote the valence band maximum and conduction band minimum, respectively.

for As-poor conditions). As these defects develop defect levels near the midgap region (Figure 8), they will act as critical SRH recombination centers. Like GeAs$_2$, SiAs$_2$ should be grown under As-rich conditions to suppress SRH recombination, retaining the Fermi level near the midgap. Overall, the influence of native defects is likely to be weaker in SiAs$_2$ than in GeAs$_2$ because of the larger defect-formation energies.

For NaSbS$_2$, most of the defects do not generate defect levels near the midgap, as shown in Figures 7e and 7f for S-rich and S-poor conditions, respectively, implying that native defects do not affect the performance of PV cells much. Only Sb interstitial (Sb$_i$) is found to create defect levels near the midgap, but it has a large formation energy, irrespective of the growth conditions. Therefore, NaSbS$_2$ is expected to be defect-tolerant.

In an earlier work,[53] defect-tolerant properties of potential PV absorbers were examined based on orbital characters of valence and conduction bands. Such simplified analysis may be acceptable for a screening purpose because full defect calculations are too demanding. However, it is difficult to rationalize this approach for a broad class of materials and various defect types.[14]

4. CONCLUSION

In conclusion, the present work is aimed at discovering indirect-gap semiconductors that are potential PV absorbers. To derive the design principles, we examined the light-to-electricity conversion process in detail. Subsequently, we explored the pre-existing computational database and performed high-throughput calculations for screening potential PV absorbers. As a result, we identified GeAs$_2$, SiAs$_2$, and NaSbS$_2$, which consist of earth-abundant and cheap elements, as promising PV absorbers. The absorption coefficients of these three compounds were examined as a function of photon energies, and the results indicated that they absorb visible light efficiently. Finally, we computed the formation energies of native point defects in these materials offering guidelines to optimize growth conditions. Among the three candidates, NaSbS$_2$ has been studied in application to PV absorbers in recent works.[17,45,54,55] Interestingly, a η_{max} value of around 3.18% was reported for a NaSbS$_2$ solar cell.[45] This efficiency is comparable to that of initial PV cells of a similar device type with organic−inorganic hybrid halide perovskites.[56] We expect that further optimization of device structures and improvement in material quality would result in a higher efficiency of such PV cells, as happened to halide perovskite solar cells. By establishing design rules for indirect-gap semiconductors for PV absorbers and proposing new materials, we believe that the present work will contribute to the development of cost-effective and high-performance PV cells.

■ ASSOCIATED CONTENT

ⓢ Supporting Information

The Supporting Information is available free of charge on the ACS Publications website at DOI: 10.1021/acs.chemmater.9b00708.

Electronic band structure of GeAs$_2$, SiAs$_2$, and NaSbS$_2$, calculated SLME, and chemical potentials for defect calculations (PDF)

■ AUTHOR INFORMATION

Corresponding Author

*E-mail: thehoya84@gmail.com.

ORCID ⦿

Youngho Kang: 0000-0003-4532-0027

Notes

The authors declare no competing financial interest.

■ REFERENCES

(1) Ellabban, O.; Abu-Rub, H.; Blaabjerg, F. Renewable Energy Resources: Current Status, Future Prospects and Their Enabling Technology. *Renewable Sustainable Energy Rev.* **2014**, *39*, 748−764.

(2) Nayak, P. K.; Garcia-Belmonte, G.; Kahn, A.; Bisquert, J.; Cahen, D. Photovoltaic Efficiency Limits and Material Disorder. *Energy Environ. Sci.* **2012**, *5*, 6022−6039.

(3) Parida, B.; Iniyan, S.; Goic, R. A Review of Solar Photovoltaic Technologies. *Renewable Sustainable Energy Rev.* **2011**, *15*, 1625−1636.

(4) Polman, A.; Knight, M.; Garnett, E. C.; Ehrler, B.; Sinke, W. C. Photovoltaic Materials: Present Efficiencies and Future Challenges. *Science* **2016**, *352*, No. aad4424.

(5) Green, M. A. Commercial Progress and Challenges for Photovoltaics. *Nat. Energy* **2016**, *1*, 15015.

(6) Eyderman, S.; Deinega, A.; John, S. Near Perfect Solar Absorption in Ultra-Thin-Film GaAs Photonic Crystals. *J. Mater. Chem. A* **2014**, *2*, 761−769.

(7) Ramanujam, J.; Singh, U. P. Copper Indium Gallium Selenide Based Solar Cells − a Review. *Energy Environ. Sci.* **2017**, *10*, 1306−1319.

(8) Green, M. A.; Ho-Baillie, A.; Snaith, H. J. The Emergence of Perovskite Solar Cells. *Nat. Photonics* **2014**, *8*, 506−514.

(9) Stranks, S. D.; Snaith, H. J. Metal-Halide Perovskites for Photovoltaic and Light-Emitting Devices. *Nat. Nanotechnol.* **2015**, *10*, 391−402.

(10) Kang, Y.; Han, S. Intrinsic Carrier Mobility of Cesium Lead Halide Perovskites. *Phys. Rev. Appl.* **2018**, *10*, 044013.

(11) Green, M. A.; Hishikawa, Y.; Dunlop, E. D.; Levi, D. H.; Hohl-Ebinger, J.; Ho-Baillie, A. W. Y. Solar Cell Efficiency Tables (version 52). *Prog. Photovoltaics* **2018**, *26*, 427−436.

(12) Leijtens, T.; Eperon, G. E.; Noel, N. K.; Habisreutinger, S. N.; Petrozza, A.; Snaith, H. J. Stability of Metal Halide Perovskite Solar Cells. *Adv. Energy Mater.* **2015**, *5*, 1500963.

(13) Park, N. G.; Grätzel, M.; Miyasaka, T.; Zhu, K.; Emery, K. Towards Stable and Commercially Available Perovskite Solar Cells. *Nat. Energy* **2016**, *1*, 16152.

(14) Kuhar, K.; Pandey, M.; Thygesen, K. S.; Jacobsen, K. W. High-Throughput Computational Assessment of Previously Synthesized

Semiconductors for Photovoltaic and Photoelectrochemical Devices. *ACS Energy Lett.* **2018**, *3*, 436−446.

(15) Yu, L.; Zunger, A. Identification of Potential Photovoltaic Absorbers Based on First-Principles Spectroscopic Screening of Materials. *Phys. Rev. Lett.* **2012**, *108*, 068701.

(16) Yu, L.; Kokenyesi, R. S.; Keszler, D. A.; Zunger, A. Inverse Design of High Absorption Thin-Film Photovoltaic Materials. *Adv. Energy Mater.* **2013**, *3*, 43−48.

(17) Fabini, D. H.; Koerner, M.; Seshadri, R. Candidate Inorganic Photovoltaic Materials from Electronic Structure-Based Optical Absorption and Charge Transport Proxies. *Chem. Mater.* **2019**, *31*, 1561−1574.

(18) Azarhoosh, P.; McKechnie, S.; Frost, J. M.; Walsh, A.; Van Schilfgaarde, M. Research Update: Relativistic origin of slow electron-hole recombination in hybrid halide perovskite solar cells. *APL Mater.* **2016**, *4*, 091501.

(19) Hutter, E. M.; Gélvez-Rueda, M. C.; Osherov, A.; Bulovic, V.; Grozema, F. C.; Stranks, S. D.; Savenije, T. J. Direct-Indirect Character of the Bandgap in Methylammonium Lead Iodide Perovskite. *Nat. Mater.* **2017**, *16*, 115−120.

(20) Jain, A.; Ong, S. P.; Hautier, G.; Chen, W.; Richards, W. D.; Dacek, S.; Cholia, S.; Gunter, D.; Skinner, D.; Ceder, G.; Persson, K. A. Commentary: The Materials Project: A Materials Genome Approach to Accelerating Materials Innovation. *APL Mater.* **2013**, *1*, 011002.

(21) Hautier, G.; Miglio, A.; Waroquiers, D.; Rignanese, G.-M.; Gonze, X. How Does Chemistry Influence Electron Effective Mass in Oxides? A High-Throughput Computational Analysis. *Chem. Mater.* **2014**, *26*, 5447−5458.

(22) Hautier, G.; Miglio, A.; Ceder, G.; Rignanese, G. M.; Gonze, X. Identification and Design Principles of Low Hole Effective Mass P-Type Transparent Conducting Oxides. *Nat. Commun.* **2013**, *4*, 2292.

(23) Kresse, G.; Fürthmuller, J. Efficient Iterative Schemes for Ab Initio Total-Energy Calculations Using a Plane-Wave Basis Set. *Phys. Rev. B: Condens. Matter Mater. Phys.* **1996**, *54*, 11169−11186.

(24) Kresse, G.; Joubert, D. From Ultrasoft Pseudopotentials to the Projector Augmented-Wave Method. *Phys. Rev. B: Condens. Matter Mater. Phys.* **1999**, *59*, 1758−1775.

(25) Perdew, J. P.; Burke, K.; Ernzerhof, M. Generalized Gradient Approximation Made Simple. *Phys. Rev. Lett.* **1996**, *77*, 3865−3868.

(26) Madsen, G. K. H.; Carrete, J.; Verstraete, M. J. BoltzTraP2, a Program for Interpolating Band Structures and Calculating Semi-Classical Transport Coefficients. *Comput. Phys. Commun.* **2018**, *231*, 140−145.

(27) Heyd, J.; Scuseria, G. E.; Ernzerhof, M. Hybrid Functionals Based on a Screened Coulomb Potential. *J. Chem. Phys.* **2003**, *118*, 8207−8215.

(28) Heyd, J.; Scuseria, G. E.; Ernzerhof, M. Erratum: "Hybrid Functionals Based on a Screened Coulomb Potential"[J. Chem. Phys. 118, 8207 (2003)]. *J. Chem. Phys.* **2006**, *124*, 219906.

(29) Grimme, S.; Antony, J.; Ehrlich, S.; Krieg, H. A Consistent and Accurate Ab Initio Parametrization of Density Functional Dispersion Correction (DFT-D) for the 94 Elements H-Pu. *J. Chem. Phys.* **2010**, *132*, 154104.

(30) Del Sole, R.; Girlanda, R. Optical Properties of Semiconductors within the Independent-Quasiparticle Approximation. *Phys. Rev. B: Condens. Matter Mater. Phys.* **1993**, *48*, 11789−11795.

(31) Shockley, W.; Queisser, H. J. Detailed Balance Limit of Efficiency of p-n Junction Solar Cells. *J. Appl. Phys.* **1961**, *32*, 510−519.

(32) Yang, Y.; Ostrowski, D. P.; France, R. M.; Zhu, K.; van de Lagemaat, J.; Luther, J. M.; Beard, M. C. Observation of a Hot-Phonon Bottleneck in Lead-Iodide Perovskites. *Nat. Photonics* **2016**, *10*, 53−59.

(33) Ren, X.; Wang, Z.; Sha, W. E.; Choy, W. C. H. Exploring the Way to Approach the Efficiency Limit of Perovskite Solar Cells by Drift-Diffusion Model. *ACS Photonics* **2017**, *4*, 934−942.

(34) Hall, R. N. Electron-Hole Recombination in Germanium. *Phys. Rev.* **1952**, *87*, 387.

(35) Shockley, W.; Read, W. T. Statistics of the Recombinations of Holes and Electrons. *Phys. Rev.* **1952**, *87*, 835−842.

(36) Yamada, Y.; Nakamura, T.; Endo, M.; Wakamiya, A.; Kanemitsu, Y. Photocarrier Recombination Dynamics in Perovskite CH3NH3PbI3 for Solar Cell Applications. *J. Am. Chem. Soc.* **2014**, *136*, 11610−11613.

(37) Alkauskas, A.; Yan, Q.; Van de Walle, C. G. First-Principles Theory of Nonradiative Carrier Capture via Multiphonon Emission. *Phys. Rev. B: Condens. Matter Mater. Phys.* **2014**, *90*, 075202.

(38) Shen, J.-X.; Wickramaratne, D.; Dreyer, C. E.; Alkauskas, A.; Young, E.; Speck, J. S.; Van de Walle, C. G. Calcium as a Nonradiative Recombination Center in InGaN. *Appl. Phys. Express* **2017**, *10*, 021001.

(39) Park, S.; Lee, B.; Jeon, S. H.; Han, S. Hybrid Functional Study on Structural and Electronic Properties of Oxides. *Curr. Appl. Phys.* **2011**, *11*, S337−S340.

(40) Koster, L. J. A.; Mihailetchi, V. D.; Ramaker, R.; Blom, P. W. M. Light Intensity Dependence of Open-Circuit Voltage of Polymer:-Fullerene Solar Cells. *Appl. Phys. Lett.* **2005**, *86*, 123509.

(41) Bercx, M.; Sarmadian, N.; Saniz, R.; Partoens, B.; Lamoen, D. *Phys. Chem. Chem. Phys.* **2016**, *18*, 20542−20549.

(42) Yim, K.; Yong, Y.; Lee, J.; Lee, K.; Nahm, H. H.; Yoo, J.; Lee, C.; Hwang, C. S.; Han, S. Novel High-κ Dielectrics for Next-Generation Electronic Devices Screened by Automated Ab Initio Calculations. *NPG Asia Mater.* **2015**, *7*, No. e190.

(43) Whalley, L. D.; Frost, J. M.; Morgan, B. J.; Walsh, A. Impact of Nonparabolic Electronic Band Structure on the Optical and Transport Properties of Photovoltaic Materials. *Phys. Rev. B: Condens. Matter Mater. Phys.* **2019**, *99*, 085207.

(44) Wadsten, T.; et al. The Crystal Structures of SiP2, SiAs2, and GeP. *Acta Chem. Scand.* **1967**, *21*, 593−594.

(45) Rahayu, S. U.; Chou, C.-L.; Suriyawong, N.; Aragaw, B. A.; Shi, J.-B.; Lee, M.-W. Sodium Antimony Sulfide (NaSbS2): Turning an Unexpected Impurity into a Promising, Environmentally Friendly Novel Solar Absorber Material. *APL Mater.* **2016**, *4*, 116103.

(46) Walsh, A.; Da Silva, J. L. F.; Wei, S. H.; Körber, C.; Klein, A.; Piper, L. F. J.; DeMasi, A.; Smith, K. E.; Panaccione, G.; Torelli, P.; Payne, D. J.; Bourlange, A.; Egdell, R. G. Nature of the Band Gap of In2O3 Revealed by First-Principles Calculations and X-Ray Spectroscopy. *Phys. Rev. Lett.* **2008**, *100*, 167402.

(47) Aspnes, D. E.; Studna, A. A. Dielectric Functions and Optical Parameters of Si, Ge, GaP, GaAs, GaSb, InP, InAs, and InSb from 1.5 to 6.0 eV. *Phys. Rev. B: Condens. Matter Mater. Phys.* **1983**, *27*, 985−1009.

(48) Freysoldt, C.; Grabowski, B.; Hickel, T.; Neugebauer, J.; Kresse, G.; Janotti, A.; Van de Walle, C. G. First-Principles Calculations for Point Defects in Solids. *Rev. Mod. Phys.* **2014**, *86*, 253−305.

(49) Freysoldt, C.; Neugebauer, J.; Van de Walle, C. G. Electrostatic Interactions between Charged Defects in Supercells. *Phys. Status Solidi B* **2011**, *248*, 1067−1076.

(50) Freysoldt, C.; Neugebauer, J.; Van de Walle, C. G. Fully Ab Initio Finite-Size Corrections for Charged-Defect Supercell Calculations. *Phys. Rev. Lett.* **2009**, *102*, 016402.

(51) Van de Walle, C. G. Hydrogen as a Cause of Doping in Zinc Oxide. *Phys. Rev. Lett.* **2000**, *85*, 1012−1015.

(52) Kang, Y.; Han, S. An Origin of Unintentional Doping in Transition Metal Dichalcogenides: the Role of Hydrogen Impurities. *Nanoscale* **2017**, *9*, 4265−4271.

(53) Brandt, R. E.; Stevanovic, V.; Ginley, D. S.; Buonassisi, T. Identifying Defect-Tolerant Semiconductors with High Minority-Carrier Lifetimes: Beyond Hybrid Lead Halide Perovskites. *MRS Commun.* **2015**, *5*, 265−275.

(54) Leung, W. W. W.; Savory, C. N.; Palgrave, R. G.; Scanlon, D. O. An Experimental and Theoretical Study into NaSbS2 as an Emerging Solar Absorber. *J. Mater. Chem. C* **2019**, *7*, 2059−2067.

(55) Sun, W. C.; Rahayu, S. U.; Lee, M. W. Eco-Friendly NaSbS2 Quantum Dot-Sensitized Solar Cells. *IEEE J. Photovoltaics* **2018**, *8*, 1011−1016.

(56) Kojima, A.; Teshima, K.; Shirai, Y.; Miyasaka, T. Organometal Halide Perovskites as Visible-Light Sensitizers for Photovoltaic Cells. *J. Am. Chem. Soc.* **2009**, *131*, 6050−6051.